to be a lipopolysaccharide (LPS) mimetic [18]. For example, paclitaxel enhances secretion of interleukin 1β (IL-1β) and tumor necrosis factor-α (TNF-α) in murine macrophages by stimulating signal pathways, such as toll-like receptor 4 (TLR4)/NF-κB, and gene expression indistinguishable from that of LPS [11]. Paclitaxel also increases the secretion of both IL-1β and TNF-α by human monocytes in vitro at drug concentrations achievable with clinical use of paclitaxel; however, the precise molecular mechanism remains unclear [1, 2].

The effect of paclitaxel on nature killer (NK) cell function appears to be quite different than that on macrophage and monocyte function. Taxanes including paclitaxel suppress NK cells in vitro [8, 9, 25]. For example, Chuang et al. [9] showed that paclitaxel inhibited the cytotoxicity of human NK cells against cell lines K562 (NK cell–sensitive erythroleukemia cell line) and OV-2774 (relatively NK cell–resistant ovarian cell line). Paclitaxel also increases cytotoxicity of NK cells [24, 41]. Tsavaris et al. [41] suggested that peripheral blood lymphocyte-derived NK cell activity increases in patients with advanced breast cancer undergoing chemotherapy with taxanes including paclitaxel. In addition, Tong et al. [39] showed that NK cytotoxicity of patients with advanced cancer did not differ before or after paclitaxel treatment. Thus, the effect of paclitaxel on NK cell activity is still controversial.

The main objective of the present study is to evaluate the effect of paclitaxel at clinically relevant concentrations (nanomole level) on cytotoxicity of purified NK cells. Here, we show for the first time that paclitaxel increases cytotoxicity of NK cells against a breast carcinoma cell line in vitro and that paclitaxel both induces NF-κB activation and increases production of perforin, which is one of the effector molecules that mediate cytotoxicity in NK cells.

Materials and methods

Reagents

Paclitaxel was purchased from the Bristol-Myers Squibb (Princeton, NJ, USA) and solubilized in RPMI 1640. Pyrrolidine dithiocarbamate (PDTC), an inhibitor of NF-κB translocation, was purchased from Sigma Chemical (St Louis, MO, USA). Perforin inhibitor concanamycin A (CMA) was purchased from Wako Pure Chemicals (Osaka, Japan).

Cells

Human breast adenocarcinoma cell line BT-474 and NK cell–sensitive erythroleukemia cell line K562 were maintained in complete medium composed of RPMI 1640 and 10% fetal bovine serum (FBS) (Sigma).

Preparation of human CD16$^+$ NK cells

Peripheral blood mononuclear cells (PBMCs) of healthy volunteers were isolated from heparinized peripheral blood by Histopaque-1077 (Sigma) density gradient centrifugation. NK cells were further purified by negative selection with magnetic beads coated with mouse monoclonal anti-CD3, anti-CD4, anti-CD14, and anti-CD19 antibodies (Dynabeads; Dynal, Oslo, Norway), resulting in CD16$^+$ NK cells with greater than 95% purity. Purity was confirmed by flow cytometric analysis with anti-CD16 monoclonal antibody (mAb) (Becton Dickinson).

Cytotoxicity assay

Cytotoxicity was determined by ^{51}Cr-release assay as described previously [19]. Briefly, target cells (1×10^6/ml) were incubated with 100 μCi ^{51}Cr for 60 min and then washed twice with complete medium to eliminate residual ^{51}Cr. The ^{51}Cr-labeled target cells (1×10^4/well) and effector cells (various cell density) were suspended in 200 µl of complete medium and incubated in a 96-well U-bottomed plate in triplicate at 37 °C. After 4 h, the radioactivity of the supernatant (100 µl) was measured by a gamma counter. The percentage of cellular cytotoxicity was calculated with the following formula: % specific lysis = (experimental cpm − spontaneous cpm) / (maximum cpm − spontaneous cpm) × 100. In some experiments, the effector cells were pretreated with 20 nM CMA for 2 h to inactive perforin [15, 16].

Fluorescence-activated cell sorting (FACS) analysis

Cell surface expression of Fas ligand was examined by a single-color immunofluorescence procedure with biotin-conjugated mouse antihuman Fas ligand antibody (Becton Dickinson) and goat antimouse IgG/FITC mAbs (Becton Dickinson). Intracellular expression of perforin was also determined by flow cytometry. Cells were examined with antihuman perforin/FITC mAbs (Ancell, Bayport, MN, USA) after fixation with 2% paraformaldehyde for 30 min and then permeabilization with 0.3% saponin for 10 min. In control samples, staining was performed with antihuman IgG/FITC mAbs (Becton Dickinson) as a negative control. The labeled cells were washed twice and then analyzed with a FACSCalibur flow cytometer (Becton Dickinson) and CELLQuest software (Becton Dickinson).

Reverse transcriptase polymerase chain reaction (RT-PCR)

Natural killer cells were incubated with various concentrations of paclitaxel (0–1,000 nM) at 37°C for 24 h and then washed with PBS (Wako) to eliminate paclitaxel. Total RNA was extracted from NK cells by the

guanidinium thiocyanate–phenol–chloroform extraction method [7]. RNA (3 μg) was reverse-transcribed to cDNA with the Superscript TM II RNaseH-reverse transcriptase system (Gibco BRL, Grand Island, NY, USA). The first strand cDNAs of perforin and glyceraldehyde-3-phosphate dehydrogenase (GAPDH) were then amplified by 35 cycles of PCR (denaturation at 94°C for 1 min, annealing at 60°C for 1 min, and extension at 72°C for 1 min) with the following specific primer sets: 5′-CGGCTCACACTCACAGG-3′ (perforin sense), 5′-CTGCCGTGGATGCCTATG-3′ (perforin antisense) [38], 5′-CCACCCATGGCAAATTCCATGGCA-3′ (GAPDH sense), and 5′-TCTAGACGGCAGGTCAGGTCCACC-3′ (GAPDH antisense). PCR products were separated on ethidium bromide–containing 1.5% agarose gels. Expected RT-PCR product sizes were 369 bp for perforin and 593 bp for GAPDH. The intensity of the perforin and GAPDH bands was estimated with NIH image version 1.62 software (NIH Division of Computer Research and Technology, Bethesda, MD, USA).

Electrophoretic mobility shift assay (EMSA)

Preparation of nuclear extracts of NK cells was performed as described previously [32]. Briefly, NK cells (5×10^6) were cocultured with various concentrations of paclitaxel for 24 h, washed once with PBS, and then collected by centrifugation. Collected NK cells were homogenized in hypotonic buffer and then incubated for 10 min on ice. Nuclei were collected by centrifugation at 800 *g* for 5 min, washed once with hypotonic buffer, and resuspended in low-salt buffer. An equal volume of high-salt buffer was added with vortex mixing. Nuclei were incubated for 30 min on ice and centrifuged at 1,800 *g* for 30 min, and the supernatants were collected. Nuclear protein extracts of NK cells were analyzed by EMSA for NF-κB nuclear translocation as described previously [32]. Briefly, nuclear protein extracts of $5–8\times10^6$ cells were incubated for 30 min at 37°C with binding buffer, poly (dI-dC) (Amersham Pharmacia Biotech, Uppsala, Sweden), and ^{32}P-labeled double-stranded oligonucleotide containing the binding motif of NF-κB (5′-AGTTGAGGGGACTTTCCCAGGC-3′; Promega, Madison, WI, USA). The sequence of Oct-1 probe was 5′-CTAGATATGCAAATCATTG-3′. These mixtures were loaded onto a 4% polyacrylamide gel and separated by electrophoresis in 0.25xTBE running buffer. The oligomer–protein complexes were visualized by autoradiography.

Statistical analysis

Student's *t* test was used for statistical analyses. All results with a *P* value less than 0.05 were considered statistically significant.

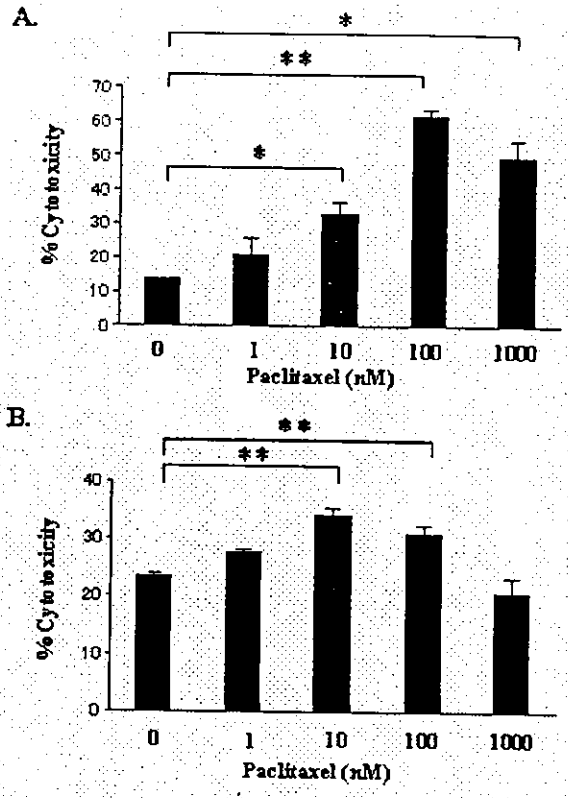

Fig. 1 Effects of paclitaxel on cytotoxicity of NK cells against BT-474 cells and K562 cells. NK cells, which were purified by negative selection with magnetic beads, were cocultured with various concentrations of paclitaxel (0–1,000 nM) at 37°C for 24 h and then washed to eliminate paclitaxel. Cytotoxicity was determined by ^{51}Cr-release assay at effector to target cell ratios of 10:1 and 5:1 (a and b, respectively). Paclitaxel enhanced cytotoxicity of NK cells against BT-474 cells and K562 cells (a and b, respectively) at relatively low concentrations. *Bars* SD. $^*P<0.05$ (significant difference from control); $^{**}P<0.01$

Results

Paclitaxel enhances cytotoxicity of NK cells

Natural killer cells were cocultured with various concentrations of paclitaxel (1–1,000 nM) at 37°C for 24 h. Then NK cells were washed twice with complete medium to eliminate residual paclitaxel and resuspended in fresh complete medium. Treatment of NK cells with paclitaxel at less than 1,000 nM did not affect cellular viability and total living cell numbers (data not shown). K562 cells are highly sensitive to NK cells, and BT-474 cells are relatively resistant to NK cells. To reveal the effect of paclitaxel on cytotoxicity of NK cells, we used effector to target ratios of 5:1 and 10:1 for K562 cells and BT-474 cells, respectively, throughout this study. Paclitaxel increased cytotoxicity of NK cells against BT-474 cells and K562 cells (Fig. 1a and b, respectively) at 1–100 nM, in

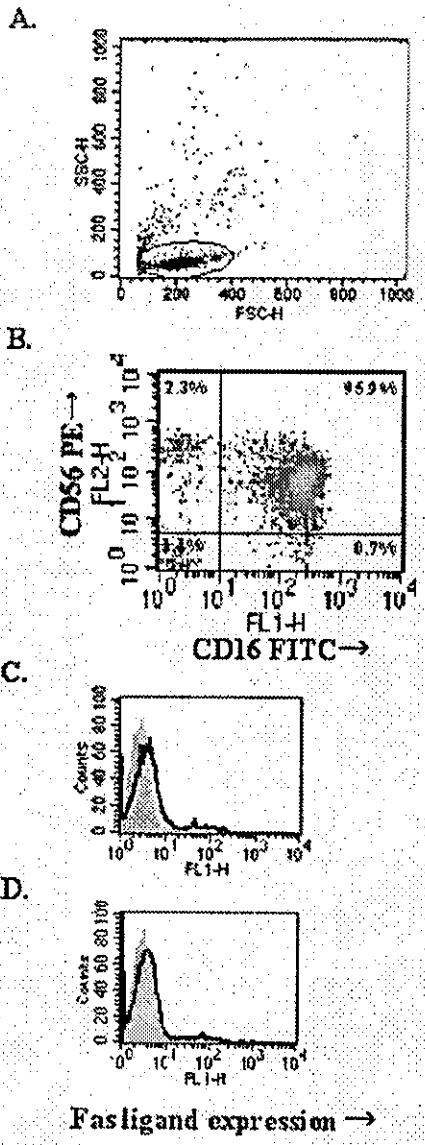

Fig. 2 Effects of paclitaxel on Fas ligand expression of NK cells. After NK cells were cultured with paclitaxel at various concentrations (0–100 nM) for 24 h, Fas ligand expression on NK cells was determined by FACS analysis. Flow cytometry was performed as described in "Materials and methods." Mean fluorescence intensity (MFI) was analyzed by CELLQuest software. **a** Representative cytogram obtained from NK cells purified by negative selection with magnetic beads and treated with 10 nM paclitaxel for 24 h is shown. *Circle* indicates lymphocytes region. **b** Purity of $CD16^+$ NK cells of gated cells (*circle*) was 96.6%. **c, d** Representative histograms (*open*) of NK cells treated with (**d**) and without (**c**) 10 nM paclitaxel are shown. *Filled histograms* indicate the staining with isotype control. Paclitaxel did not affect expression of Fas ligand. Similar results were obtained with NK cells from five different healthy volunteers

a dose-dependent manner. Similar results were obtained in 12 independent experiments with NK cells from five different healthy volunteers. Representative data are shown in Fig. 1.

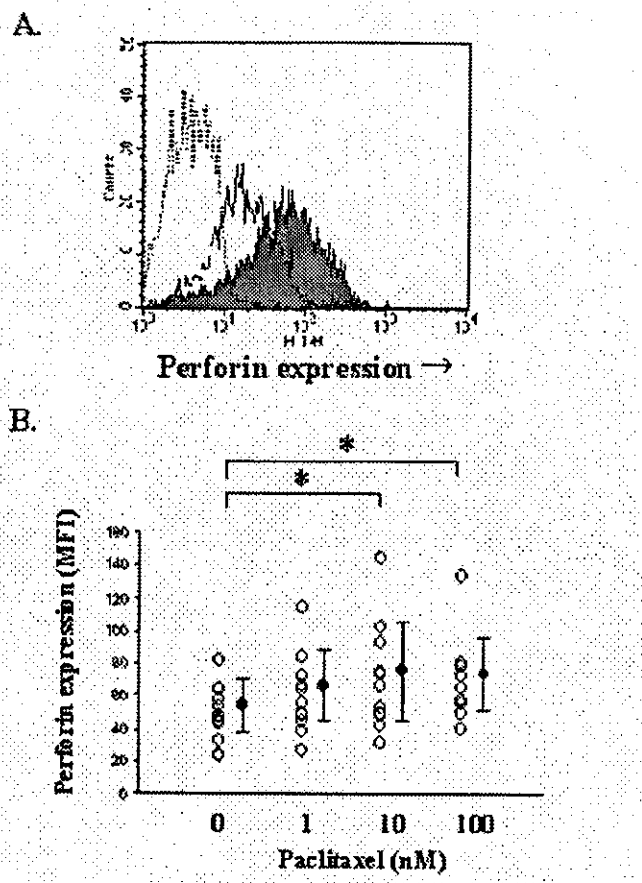

Fig. 3 Effects of paclitaxel on perforin expression of NK cells. NK cell perforin expression was determined by FACS analysis as described in Fig. 2 and "Materials and methods." **a** An *open* and *filled histogram* of perforin protein expression are indicated for nontreated NK cells and paclitaxel (10 nM) pretreated NK cells, respectively. *Dotted histogram* indicates the staining with isotype control. **b** Results from five healthy individuals showed peak perforin expression at 10–100 nM paclitaxel. *Bars* SD. $*P < 0.05$ (signifigant difference from control)

Paclitaxel does not affect Fas ligand expression of NK cells

Because two main mechanisms in NK cell cytotoxicity—i.e., the Fas/Fas ligand pathway and perforin/granzyme pathway—have generally been accepted, we first examined the effect of paclitaxel on Fas ligand expression on NK cells. NK cells treated with paclitaxel (1–100 nM) for 24 h did not affect expression of Fas ligand. A representative histogram of NK cells treated with 10 nM paclitaxel is shown in Fig. 2c, d. Similar results were obtained with NK cells from five different healthy volunteers.

Paclitaxel induces perforin production in NK cells

We next examined whether paclitaxel-induced NK cell cytotoxicity is related to perforin production. First, intracellular expression of perforin in NK cells was

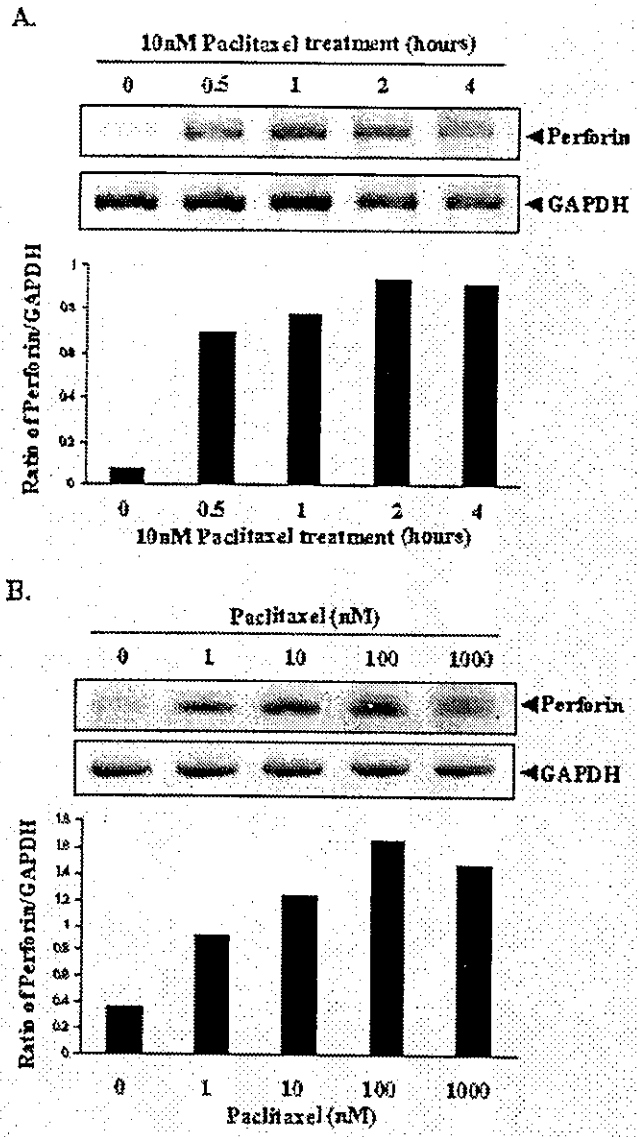

Fig. 4 Effects of paclitaxel on transcription of perforin mRNA in NK cells. **a** NK cells (2×10^6) were cultured with 10 nM paclitaxel at 37°C for various numbers of hours and then washed to eliminate paclitaxel. **b** NK cells were cultured with paclitaxel in various concentrations (0–1,000 nM) at 37°C for 4 h and then washed with PBS to eliminate paclitaxel. Transcription of perforin mRNA in NK cells was examined by RT-PCR. The level of perforin expression was quantified by densitometric scanning using NIH image software. GAPDH protein was blotted as a control

determined by FACS analysis as described in "Materials and Methods." A representative histogram of NK cells treated with 10 nM paclitaxel is shown in Fig. 3a (filled histogram). NK cells treated with paclitaxel (1–100 nM) for 24 h showed up-regulated intracellular expression of perforin in a dose-dependent manner (Fig. 3b). Similar results were obtained with NK cells from five different healthy volunteers.

Next, we examined the effect of paclitaxel on transcription of perforin mRNA in NK cells by RT-PCR. Paclitaxel increased transcription of perforin mRNA within 30 min after initial treatment and that increase continued for at least 4 h (Fig. 4a). When NK cells were treated with indicated concentrations of paclitaxel for 4 h, paclitaxel increased transcription of NK cell perforin mRNA in a dose-dependent manner (Fig. 4b). Similar results were obtained in five independent experiments with NK cells from three different healthy volunteers.

Paclitaxel induces NF-κB activation in NK cells

To examine why paclitaxel increases perforin expression of NK cells, we speculated that perforin expression is related to the NF-κB pathway. When NK cells were treated with 10 nM paclitaxel, increased nuclear translocation of NF-κB p65 was induced within 30 min after the initial culture (Fig. 5), indicating activation of NF-κB. Specificity of DNA binding was confirmed by a competition study with a 100-fold excess of unlabeled NF-κB oligonucleotide.

PDTC suppresses perforin production of NK cells induced by paclitaxel

First, the inhibitory effect of pyrrolidine dithiocarbamate (PDTC) on paclitaxel-induced NF-κB activation was confirmed. PDTC (10 μM) was added to NK cell cultures 1 h before treatment with 10 nM paclitaxel. Within 4 h, PDTC suppressed the nuclear translocation of NF-κB but not of Oct-1 (Fig. 6a). Similar results were obtained in five independent experiments with NK cells from three different healthy volunteers. Similarly, NK cells were pretreated with 10 μM PDTC for 1 h, and then 10 nM paclitaxel for 4 h to measure perforin mRNA expression, or for 24 h to measure perforin protein expression. PDTC suppressed perforin production at both mRNA and protein levels (Fig. 6b, c). Treatment of NK cells with 10 μM PDTC did not affect cellular viability and total living cell numbers (data not shown). Similar results were obtained in three independent experiments with NK cells from three different healthy volunteers.

PDTC suppresses cytotoxicity of NK cells

The NK cells were cultured with 10 nM paclitaxel with or without 10 μM PDTC at 37°C for 24 h. PDTC completely inhibited cytotoxicity of not only paclitaxel-treated NK cells but also nontreated NK cells against BT-474 cells and K562 cells (Fig. 7a, b, respectively). Treatment of NK cells with 10 μM PDTC did not affect cellular viability and total living cell numbers (data not shown). Similar results were obtained in five independent experiments with NK cells from three different healthy volunteers.

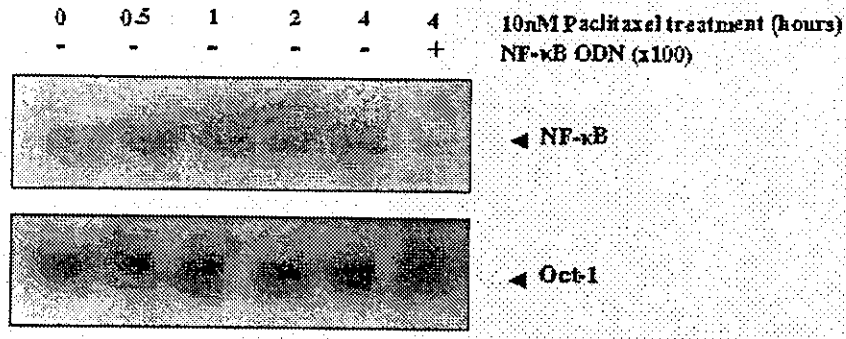

Fig. 5 Activation of NF-κB in NK cells treated with paclitaxel. Nuclear translocation of NF-κB was examined by EMSA. When NK cells were treated with 10 nM paclitaxel, NF-κB DNA binding increased within 30 min after the initial culture. In a competition study, nuclear extracts were preincubated with a 100-fold excess of unlabeled NF-κB oligonucleotide for 1 h and then with radiolabeled double-stranded oligonucleotide probe. Oct-1 protein was blotted as a control. Paclitaxel induced NF-κB activation in NK cells

CMA suppresses cytotoxicity of NK cells

The NK cells were incubated with or without 10 nM paclitaxel for 24 h. These NK cells were washed to eliminate paclitaxel and then pretreated with 20 nM CMA for 2 h before incubation with the target cells in the presence of CMA. CMA suppressed cytotoxicity of both nontreated NK cells and paclitaxel-treated NK cells against BT-474 cells and K562 cells (Fig. 8a, b, respectively). Treatment of NK cells with 20 nM CMA did not affect cellular viability and total living cell numbers (data not shown). Similar results were obtained in three independent experiments with NK cells from three different healthy volunteers.

Discussion

We provide evidence that paclitaxel at drug concentrations achievable in clinical settings can increase in vitro perforin production of NK cells and cause increased cytotoxicity against not only NK cell–sensitive K562 cells but also relatively NK cell–resistant breast carcinoma BT-474 cells. We also indicate that paclitaxel-mediated perforin production may be related to paclitaxel-induced NF-κB activation.

Paclitaxel increased perforin production at both mRNA and protein levels in NK cells, increasing their cytotoxicity (Fig. 1). Results from previous studies suggest there are two major mechanisms of NK-mediated cytotoxicity: the perforin/granzymes pathway [34, 40] and the Fas/Fas ligand pathway [26]. Since, paclitaxel did not induce a significant change in Fas ligand expression of NK cells (Fig. 2), we focused on the effect of paclitaxel on perforin-mediated cytotoxicity of NK cells. CMA is known to be a specific inhibitor of vacuolar type H^+-ATPase [46]. CMA inhibits the activity of perforin in dense granules, mostly because perforin degradation is accelerated by an increase in the pH of the lytic granules [14]. It has been postulated that CMA is a selective inhibitor, blocking only the perforin-based cytotoxicity and not affecting the Fas-based cytotoxicity [15]. Thus, in the present study, we used CMA to help determine the mechanism of paclitaxel-

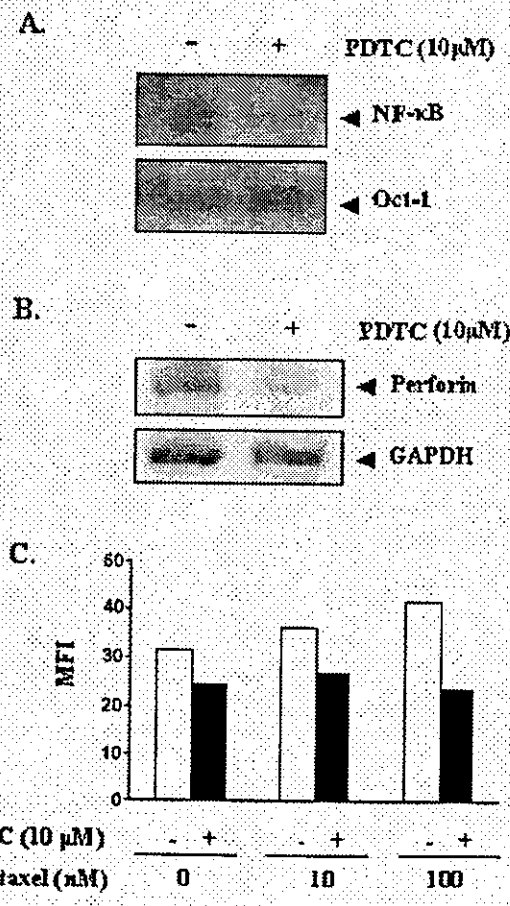

Fig. 6 Effects of NF-κB inhibitor PDTC on perforin expression in NK cells teated with paclitaxel. NK cells were pretreated with 10 μM PDTC for 1 h, and then with paclitaxel for 4 h to analyze NF-κB activation by EMSA, or for 24 h to analyze intracellular perforin expression by FACS. a PDTC suppressed the nuclear translocation of NF-κB but not of Oct-1. b, c PDTC suppressed perforin production at both mRNA and protein levels, respectively

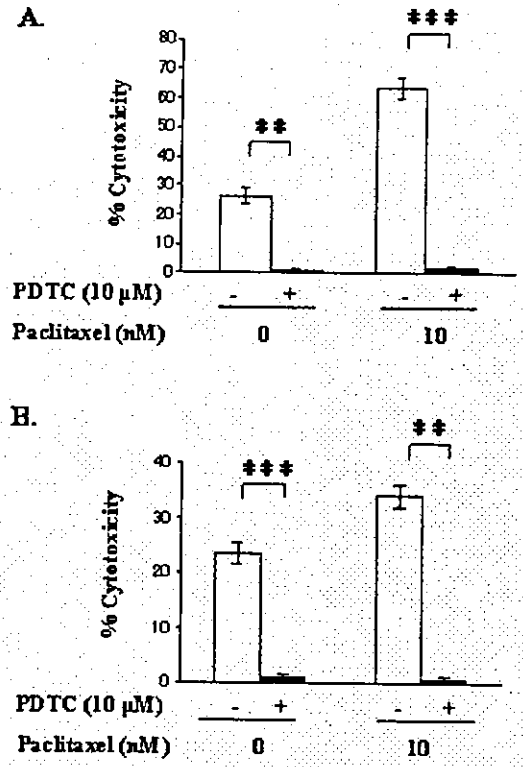

Fig. 7 Effects of PDTC on cytotoxicity of NK cells treated with paclitaxel. NK cells were pretreated with 10 μM PDTC for 1 h and then 10–100 nM paclitaxel for 24 h. Cytotoxicity was determined by ^{51}Cr-release assay at effector to target cell ratios of 10:1 (a) and 5:1 (b). Cytotoxicity of NK cells treated with or without paclitaxel against BT-474 cells (a) and K562 cells (b) was completely suppressed by PDTC. *Bars* SD. $^{**}P < 0.01$ (significant difference from control); $^{***}P < 0.001$

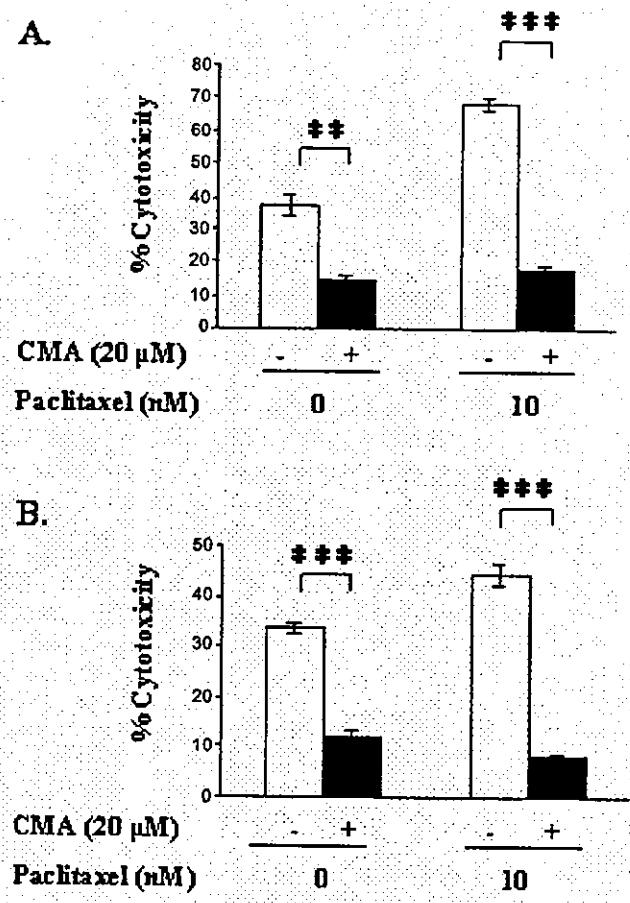

Fig. 8 Effects of perforin inhibitor CMA on cytotoxicity of NK cells treated with paclitaxel. Cytotoxicity was determined by ^{51}Cr-release assay at effector to target cell ratios of 10:1 (a) and 5:1 (b). NK cells were cultured with or without 10 nM paclitaxel at 37°C for 24 h and then washed to eliminate paclitaxel. These NK cells were treated with 20 nM CMA for 2 h before being cocultured with the target cells. BT-474 cells (a) and K562 cells (b). *Bars* SD; $^{**}P < 0.01$ (significant difference from control); $^{***}P < 0.001$

dependent cytotoxicity of perforin. CMA treatment suppressed cytotoxicity of both nontreated NK cells and paclitaxel-treated NK cells (Fig. 7). However, CMA could not completely inhibit paclitaxel-dependent cytotoxicity of NK cells. Although our present data indicate no significant role of Fas ligand in paclitaxel-induced NK cell cytotoxicity (Fig. 2), we can not rule out the existence of other cytotoxic pathways including the Fas/Fas ligand pathway. The perforin/granzymes pathway likely involves the formation of pores between NK cells and target cells by extracellular calcium-dependent polymerization of perforin. Consequently, granzymes, serin proteases responsible for downstream caspase activation, and DNA fragmentation are released into the target cell, resulting in target cell apoptosis [34, 40]. In the present study, we have data indicating that paclitaxel also induces granzyme expression of NK cells at both mRNA and protein levels (data not shown). However, the biological function of granzyme serine proteases released with perforin from the cytotoxic granules of NK cells is still controversial. Thus, it is not clear whether granzymes A and B play an essential role in cytotoxicity mediated by the perforin pathway [37]. Nonetheless, our study shows that perforin plays an important role in paclitaxel-dependent cytotoxicity of NK cells (Fig. 8).

How paclitaxel can induce increased perforin production in NK cells is an interesting question. Others showed signaling that indicated that the levels of perforin expression of NK cells are essentially controlled by IL-2Rβ [28, 31, 48]. Interestingly, DNA-binding activity of NF-κB can be induced by IL-2R signaling in T cells [5]. Valle Blázquez et al. [42] reported on a pharmacological inhibitor of NF-κB–impaired NK cell–mediated cytotoxicity. It was shown recently that NF-κB plays a critical role in perforin expression in NK cells [49]. In the present study, we used PDTC to examine the contribution of the NF-κB pathway to perforin production induced with paclitaxel. PDTC is a stable analog of dithiocarbamates and is one of the most widely used inhibitors of NF-κB signaling [4]. PDTC suppressed perforin production at both mRNA and protein levels (Fig. 6a, c). Thus, our

results strongly suggest that NF-κB plays a key role in paclitaxel-induced perforin production.

So, how does paclitaxel induce NF-κB activation in NK cells? In a murine system, paclitaxel induces NF-κB activation through TLR 4 [17]. We examined the expression of TLR 4 on NK cells by FACS analysis. Because we could not detect expression of TLR 4 on the cellular surface of either nontreated or paclitaxel-treated NK cells (data not shown), it is unclear whether activation of paclitaxel-dependent NF-κB is related to interaction between paclitaxel and TLR 4 in the human system as well.

Pyrrolidine dithiocarbamate completely inhibited not only paclitaxel-dependent NK cell–mediated cytotoxicity but also nontreated NK cell–mediated cytotoxicity (Fig. 7). Although PDTC completely inhibited paclitaxel-dependent perforin expression, PDTC did not affect intracellular levels of perforin in nontreated NK cells (Fig. 6c). As described above, the perforin/granzymes pathway is one of several cytotoxic pathways of NK cells. Binding of NK cells with target cells initiates a series of biochemical events responsible for the redistribution and secretion of granules such as perforin. Specific protein kinases (the primary kinases being Src family kinases and Syk) are central to NK cell functions, including granule release. Moreover, intervention to granule redistribution and release after target cell binding are regulated by members of the mitogen-activated protein kinase family, specifically extracellular signal-regulated kinase and p38 [29]. These molecules are directly or indirectly related to the NF-κB pathway through phosphorylation of IκB kinase [20, 27].

The detailed mechanism by which paclitaxel increases NK cell cytotoxicity is not clear. Nonetheless, our new findings are likely to be useful for future cancer treatment. A recent study showed that patients with HER-2/neu-positive breast carcinoma responded better to a combination therapy with taxanes, including paclitaxel, and a mAb against HER-2, than with either agent alone [35]. NK cells undoubtedly play an important role in this anti-HER-2 antibody therapy by a mechanism involving antibody-dependent cellular cytotoxicity [36]. Thus, understanding the effects of paclitaxel on NK cell–mediated cytotoxicity is likely to be important for developing new therapeutic strategies with taxanes.

Acknowledgements We thank Kaori Nomiyama for skillful technical assistance. This research work was supported by grants (to M. K.) for scientific research (13470240) from the Ministry of Education, Science, and Culture of Japan.

References

1. Allen JN, Moore SA, Wewers MD (1993) Taxol enhances but does not induce interleukin-1 beta and tumor necrosis factor-alpha production. J Lab Clin Med 122:374–381
2. Bacus SS, Gudkov AV, Lowe M, Lyass L, Yung Y, Komarov AP, Keyomarsi K, Yarden Y, Seger R (1992) Taxol, a microtubule-stabilizing antineoplastic agent, induces expression of tumor necrosis factor-alpha and interleukin-1 in macrophages. J Leukoc Biol 52:119–121
3. Bacus SS, Gudkov AV, Lowe M, Lyass L, Yung Y, Komarov AP, Keyomarsi K, Yarden Y, Seger R (2001) Taxol-induced apoptosis depends on MAP kinase pathways (ERK and p38) and is independent of p53. Oncogene 20:147–155
4. Baeuerle PA, Henkel T (1994) Function and activation of NF-κB in the immune system. Annu Rev Immunol 12:141–179
5. Brach MA, Gruss HJ, Riedel D, Mertelsmann R, Herrmann F (1992) Activation of NF-kappa B by interleukin 2 in human blood monocytes. Cell Growth Differ 3:421–427
6. Chevallier B, Fumoleau P, Kerbrat P, Dieras V, Roche H, Krakowski I, Azli N, Bayssas M, Lentz MA, Van Glabbeke M (1995) Docetaxel is a major cytotoxic drug for the treatment of advanced breast cancer: a phase II trial of the Clinical Screening Cooperative Group of the European Organization of Research and Treatment of Cancer. J Clin Oncol 13:314–322
7. Chomczynski P, Sacchi N (1987) Single-step method of RNA isolation by acid guanidinium thiocyanate-phenol-chloroform extraction. Anal Biochem 162:156–159
8. Chuang LT, Lotzová E, Cook KR, Cristofaroni P, Morris M, Wharton JT (1993) Effect of new investigational drug taxol on oncolytic activity and stimulation of human lymphocytes. Gynecol Oncol 49:291–298
9. Chuang LT, Lotzová E, Heath J, Cook KR, Munkarah A, Morris M, Wharton JT (1994) Alteration of lymphocyte microtubule assembly, cytotoxicity, and activation by the anticancer drug taxol. Cancer Res 54:1286–1291
10. Gelmon K (1994) The taxoids: paclitaxel and docetaxel. Lancet 344:1267–1272
11. Hayakawa M, Miyashita H, Sakamoto I, Kitagawa M, Tanaka H, Yasuda H, Karin M, Kikugawa K (2003) Evidence that reactive oxygen species do not mediate NF-κB activation. EMBO J 22:3356–3366
12. Holmes FA, Walters RS, Theriault RL, Forman AD, Newton LK, Raber MN, Buzdar AU, Frye DK, Hortobagyi GN (1991) Phase II trial of Taxol, active drug in the treatment of metastatic breast cancer. J Natl Cancer Inst 83:1797–1805
13. Huang Y, Johnson KR, Norris JS, Fan W (2000) Nuclear factor-κB/IκB signaling pathway may contribute to the mediation of paclitaxel-induced apoptosis in solid tumor cells. Cancer Res 60:4426–4432
14. Kataoka T, Takaku K, Magae J, Shinohara N, Takayama H, Kondo S, Nagai K (1994) Acidification is essential for maintaining the structure and function of lytic granules of CTL. J Immunol 153:3938–3947
15. Kataoka T, Shinohara N, Takayama H, Takaku K, Kondo S, Yonehara S, Nagai K (1996) Concanamycin A, a powerful tool for characterization and estimation of contribution of perforin- and Fas-based lytic pathways in cell-mediated cytotoxicity. J Immunol 156:3678–3686
16. Kataoka T, Yamada A, Bando M, Honma T, Mizoue K, Nagai K (2000) FD-891, a structural analogue of concanamycin A that does not affect vacuolar acidification or perforin activity, yet potently prevents cytotoxic T lymphocyte-mediated cytotoxicity through the blockage of conjugate formation. Immunol 100:170–177
17. Kawasaki K, Akashi S, Shimazu R, Yoshida T, Miyake K, Nishijima M (2000) Mouse toll-like receptor 4/MD-2 complex mediates lipopolysaccharide-mimetic signal transduction by Taxol. J Biol Chem 275:2251–2254
18. Kawasaki K, Nogawa H, Nishijima M (2003) Identification of mouse MD-2 residues important for forming the cell surface TLR4-MD-2 complex recognized by anti-TLR4-MD-2 antibodies, and for conferring LPS and Taxol responsiveness on mouse TLR4 by alanine-scanning mutagenesis. J Immunol 170:413–420
19. Kubo M, Morisaki T, Kuroki H, Tasaki A, Yamanaka N, Matsumoto K, Nakamura K, Onishi H, Baba E, Katano M (2003) Combination of adoptive immunotherapy with Her-

ceptin for patients with HER2-expressing breast cancer. Anticancer Res 23:4443–4450
20. Lee FS, Peters RT, Dang LC, Maniatis T (1998) MEKK1 activates both IκB kinase α and IκB kinase β. Proc Natl Acad Sci U S A 95:9319–9324
21. Lee LF, Li G, Templeton DJ, Ting JP (1998) Paclitaxel (Taxol)-induced gene expression and cell death are both mediated by the activation of c-Jun NH2-terminal kinase (JNK/SAPK). J Biol Chem 273:28253–28260
22. Manfredi JJ, Parness J, Horwitz SB (1982) Taxol binds to cellular microtubules. J Cell Biol 94:688–696
23. McGuire WP, Rowinsky EK, Rosenshein NB, Grumbine FC, Ettinger DS, Armstrong DK, Donehower RC (1989) Taxol: a unique antineoplastic agent with significant activity in advanced ovarian epithelial neoplasms. Ann Intern Med 111:273–279
24. Mehta S, Blackinton D, Manfredi M, Rajaratnam D, Kouttab N, Wanebo H (1997) Taxol pretreatment of tumor targets amplifies natural killer cell mediated lysis. Leuk Lymphoma 26:67–76
25. Munkarah A, Chuang L, Lotzová E, Cook K, Morris M, Wharton JT (1994) Comparative studies of taxol and taxotere on tumor growth and lymphocyte function. Gynecol Oncol 55:211–216
26. Nagata S, Golstein P (1995) The Fas death factor. Science 267:1449–1456
27. Nakano H, Shindo M, Sakon S, Nishinaka S, Mihara M, Yagita H, Okumura K (1998) Differential regulation of IκB kinase α and β by two upstream kinases, NF-κB-inducing kinase and mitogen-activated protein kinase/ERK kinase kinase-1. Proc Natl Acad Sci U S A 95:3537–3542
28. Nelson BH, Willerford DM (1998) Biology of the interleukin-2 receptor. Adv Immunol 70:1–81
29. Perussia B (2000) Signaling for cytotoxicity. Nat Immunol 1:372–374
30. Rowinsky EK, Cazenave LA, Donehower RC (1990) Taxol: a novel investigational antimicrotubule agent. J Natl Cancer Inst 82:1247–1257
31. Salcedo TW, Azzoni L, Wolf SF, Perussia B (1993) Modulation of perforin and granzyme messenger RNA expression in human natural killer cells. J Immunol 151:2511–2520
32. Sasaki N, Morisaki T, Hashizume K, Yao T, Tsuneyoshi M, Noshiro H, Nakamura K, Yamanaka T, Uchiyama A, Tanaka M, Katano M (2001) Nuclear factor-κB p65 (RelA) transcription factor is constitutively activated in human gastric carcinoma tissue. Clin Cancer Res 7:4136–4142
33. Schiff PB, Fant J, Horwitz SB (1979) Promotion of microtubule assembly in vitro by taxol. Nature 277:665–667
34. Shresta S, Heusel JW, Macivor DM, Wesselschmidt RL, Russell JH, Ley TJ (1995) Granzyme B plays a critical role in cytotoxic lymphocyte-induced apoptosis. Immunol Rev 146:211–221
35. Slamon DJ, Leyland-Jones B, Shak S, Fuchs H, Paton V, Bajamonde A, Fleming T, Eiermann W, Wolter J, Pegram M, Baselga J, Norton L (2001) Use of chemotherapy plus a monoclonal antibody against HER2 for metastatic breast cancer that overexpresses HER2. N Engl J Med 344:783–792
36. Sliwkowski MX, Lofgren JA, Lewis GD, Hotaling TE, Fendly BM, Fox JA (1999) Nonclinical studies addressing the mechanism of action of trastuzumab (Herceptin). Semin Oncol 26:60–70
37. Smyth MJ, Street SEA, Trapani JA (2003) Granzymes A and B are not essential for perforin-mediated tumor rejection. J Immunol 171:515–518
38. Strehlau J, Pavlakis M, Lipman M, Shapiro M, Vasconcellos L, Harmon W, Strom TN (1997) Quantitative detection of immune activation transcripts as a diagnostic tool in kidney transplantation. Proc Natl Acad Sci U S A 94:695–700
39. Tong AW, Seamour B, Lawson JM, Ordonez G, Vukelja S, Hyman W, Richards D, Stein L, Maples PB, Nemunaitis J (2000) Cellular immune profile of patients with advanced cancer before and after taxane treatment. Am J Clin Oncol 23:463–472
40. Trapani JA, Smyth MJ (2002) Functional significance of the perforin/granzyme cell death pathway. Nat Rev Immunol 2:735–747
41. Tsavaris N, Kosmas C, Vadiaka M, Kanelopoulos P, Boulamatsis D (2002) Immune changes in patients with advanced breast cancer undergoing chemotherapy with taxanes. Br J Cancer 87:21–27
42. Valle Blázquez M, Luque I, Collantes E, Aranda E, Solana R, Peña J, Muñoz E (1997) Cellular redox status influences both cytotoxic and NF-κB activation in natural killer cells. Immunology 90:455–460
43. Wahl AF, Donaldson KL, Fairchild C, Lee FYF, Foster SA, Demers GW, Galloway DA (1996) Loss of normal p53 function confers sensitization to Taxol by increasing G2/M arrest and apoptosis. Nat Med 2:72–79
44. Wang TH, Popp DM, Wang HS, Saitoh M, Mural JG, Henley DC, Ichijo H, Wimalasena J (1999) Microtubule dysfunction induced by paclitaxel initiates apoptosis through both c-Jun N-terminal kinase (JNK)-dependent and -independent pathways in ovarian cancer cells. J Biol Chem 274:8208–8216
45. Woo JT, Shinohara C, Sakai K, Hasumi K, Endo A (1992) Isolation, characterization and biological activities of concanamycins as inhibitors of lysosomal acidification. J Antibiot (Tokyo) 45:1108–1116
46. Yamamoto K, Ichijo H, Korsmeyer SJ (1999) BCL-2 is phosphorylated and inactivated by an ASK1/Jun N-terminal protein kinase pathway normally activated at G_2/M. Mol Cell Biol 19:8469–8478
47. Yang CP, Horwitz SB (2000) Taxol mediates serine phosphorylation of the 66-kDa Shc isoform. Cancer Res 60:5171–5178
48. Zhang BJ, Scordi I, Smyth MJ, Lichtenheld MG (1999) Interleukin 2 receptor signaling regulates the perforin gene through signal transducer and activator of transcription (Stat) 5 activation of two enhancers. J Exp Med 190:1297–1307
49. Zhou J, Zhang J, Lichtenheld MG, Meadows GG (2002) A role for NF-κB activation in perforin expression of NK cells upon IL-2 receptor signaling. J Immunol 169:1319–1325

ELSEVIER

Journal of Immunological Methods 287 (2004) 79–90

JIM
Journal of Immunological Methods

www.elsevier.com/locate/jim

Research Paper

Three-dimensional two-layer collagen matrix gel culture model for evaluating complex biological functions of monocyte-derived dendritic cells

Akira Tasaki[a], Naoki Yamanaka[a], Makoto Kubo[a], Kotaro Matsumoto[a], Hideo Kuroki[a], Katsuya Nakamura[a], Chihiro Nakahara[a], Hideya Onishi[a], Hirotaka Kuga[a], Eishi Baba[a], Masao Tanaka[b], Takashi Morisaki[a], Mitsuo Katano[a,*]

[a] *Department of Cancer Therapy and Research, Graduate School of Medical Sciences, Kyushu University, 3-1-1 Maidashi, Higashi-ku, Fukuoka 812-8525, Japan*

[b] *Department of Clinical Oncology, Graduate School of Medical Sciences, Kyushu University, 3-1-1 Maidashi, Higashi-ku, Fukuoka 812-8525, Japan*

Received 28 July 2003; received in revised form 20 January 2004; accepted 21 January 2004

Abstract

Dendritic cell-like cells (Mo-DCs) generated from peripheral blood monocytes with interleukin-4 (IL-4) and granulocyte-macrophage colony-stimulating factor (GM-CSF) have been used as tools to treat cancer patients (DC-vaccines). Because Mo-DCs have multiple antigen presentation-related functions, including phagocytosis, migration, cytokine production, and T cell stimulation, establishment of a method for simultaneously evaluating the various functions of Mo-DCs is important. We developed a new in vitro three-dimensional two-layer collagen matrix culture model that consists of a collagen gel containing Mo-DCs as the lower layer and a collagen gel containing necrotic GCTM-1 tumor cells and/or T cells as the upper layer. We used this system to observe simultaneously multiple functions of Mo-DCs by phase-contrast or fluorescence microscopy and to assess IL-12 secretion during more than 2 weeks of culture. We also observed interactions between Mo-DCs and necrotic GCTM-1 or T cells on an individual cell basis by time-lapse videomicroscopy. In addition, we collected Mo-DCs from the collagen gels by collagenase treatment and analyzed the expression of antigen presentation-related molecules such as HLA-DR, CD80, CD83, and CD86 on Mo-DCs. This model may be a useful tool for evaluation of the various functions of Mo-DCs used as DC vaccines and for studies of the complex behaviors of Mo-DCs in vivo.

Keywords: Mo-DC; Collagen matrix; Migration; Phagocytosis; IL-12 production

Abbreviations: DCs, dendritic cells; Mo-DCs, dendritic cell-like cells; IL, interleukin; MHC, major histocompatibility complex; GM-CSF, granulocyte macrophage colony stimulating factor; PBMCs, peripheral blood mononuclear cells; FBS, fetal bovine serum; PBS, phosphate-buffered saline; HSA, human serum albumin; BSA, bovine serum albumin; IFN-γ, Interferon-γ; ELISA, enzyme-linked immunosorbent assay; PI, propidium iodide; 2-D, two-dimensional; 3-D, three-dimensional.

* Corresponding author. Tel.: +81-92-642-6219; fax: +81-92-642-6221.
E-mail address: mkatano@tumor.med.kyushu-u.ac.jp (M. Katano).

0022-1759/$ - see front matter © 2004 Elsevier B.V. All rights reserved.
doi:10.1016/j.jim.2004.01.014

1. Introduction

Dendritic cells (DCs) are found in most tissues, and they capture and process antigens and display large amounts of MHC-peptide complexes on their surfaces (Banchereau and Steinman, 1998; Banchereau et al., 2000). Because DCs display both MHC-class II molecules and co-stimulatory molecules such as CD80 and CD86, only DCs can induce primary sensitization against specific antigens in naïve T cells (Lanzavecchia and Sallusto, 2001). It is generally accepted that dendritic cell-like cells (monocyte-derived dendritic cells, Mo-DCs) are induced from peripheral blood mononuclear cells (PBMCs) by granulocyte-macrophage colony-stimulating factor (GM-CSF) and interleukin-4 (IL-4) in vitro (Sallusto and Lanzavecchia, 1994). Mo-DCs have many features similar to those of primary DCs, including antigen capture, co-expression of co-stimulatory molecules with MHC molecules, and secretion of IL-12 (Cella et al., 1997). It has been suggested that Mo-DCs, injected intradermally or subcutaneously, capture and process antigens, move to the T cell-dependent areas of secondary lymphoid organs, and stimulate naïve T cells (Thomas et al., 1999; Thurner et al., 1999). In this capacity, Mo-DCs have been utilized as vectors for vaccine therapies against various cancers (Dallal and Lotze, 2000; Fong and Engleman, 2000; Banchereau et al., 2001; Reinhard et al., 2002; Schuler et al., 2003).

Several problems must be addressed to evaluate DC function for vaccine therapy. First, most data concerning the antigen-presenting ability of Mo-DCs have been obtained with PBMCs from healthy donors, not cancer patients. Recent studies have indicated that Mo-DCs from advanced cancer patients are impaired at several stages of the antigen-presenting process (Onishi et al., 2002), suggesting that the antigen-presentation-related functions of individual Mo-DCs used for vaccine therapies must be evaluated closely. A second problem is that very little is known about the biological behaviors of Mo-DCs administered to cancer patients.

Three-dimensional (3-D) hydrated collagen lattices have been widely used for in vivo-like culture of various types of cells including tumor cells, lymphoid cells, and DCs (Friedl et al., 1993, 1995; Gunzer et al., 1997; Nakamura et al., 2002) because many studies have shown that the fiber distribution and biophysical architecture of collagen lattices closely resemble interstitial soft tissues, dermis, and network-like stroma of the lymph node (Friedl et al., 1998; Friedl and Brocker, 2000; Gunzer et al., 2000b). For example, Gunzer et al. (1997) developed a unique method to analyze individual DC migration within a 3-D collagen lattice. However, these complicated methods are difficult for evaluating the antigen-presenting ability of Mo-DCs used in DC-vaccine therapies.

Mo-DCs are characterized by a high rate of antigen uptake in the immature state and high antigen-presenting function (surface marker and cytokine production) in the mature state. To capture antigens, Mo-DCs have to migrate toward antigens. In addition, antigen-capturing Mo-DCs mature, then move to the T-dependent areas of secondary lymphoid organs, and stimulate naïve T-cells. In conventional monolayer culture system, we must evaluate various kinds of Mo-DC's functions by an individual method. We describe here a novel method to evaluate the quality of Mo-DCs used for cancer therapy. Our 3-D model consists of two collagen gel layers: a lower layer containing Mo-DCs and an upper layer containing necrotic tumor cells or necrotic tumor cells and T cells. In our model, GCTM-1-capturing Mo-DCs mean that Mo-DCs moved toward necrotic GCTM-1 and captured them. And increase of surface marker such as HLA-DR and CD80 indicates maturation of Mo-DCs. Increase of IL-12 production by Mo-DCs indicates activation of Mo-DCs. In addition, IFN-γ production by CD4+ T cells indicates ability of CD4+ T cell activation by Mo-DCs. By our two-layer culture system, we can estimate various kinds of Mo-DC's functions at a time. Interestingly, phase-contrast microscopy allowed us to analyze several Mo-DCs functions, including migration, antigen capture, phagocytosis, and cytokine secretion, in this system in real time. In the future, video microscopy may allow us to analyze in vivo-like behaviors of Mo-DCs.

2. Materials and methods

2.1. Generation of Mo-DCs

Mo-DCs were generated from the adherent fraction of PBMCs of healthy volunteers as previously de-

scribed but with minor modifications (Kuppner et al., 2001). In brief, PBMCs were isolated from heparinized peripheral blood by Histopaque-1077 (Sigma, St. Louis, MO) density gradient centrifugation. PBMCs were resuspended in RPMI 1640 basal medium (Sanko Pure Chemicals, Tokyo, Japan) supplemented with 10% fetal bovine serum (FBS; Filtron, Australia), 100 μg/ml penicillin (Meijiseika, Tokyo, Japan), and 100 μg/ml streptomycin (Meijiseika), plated at a density of 2×10^6 cells/ml, and allowed to adhere in 24-well culture plates (Nalge Nunc International, Chiba, Japan) overnight at 37 °C. The nonadherent cells were then removed, and the adherent cells were harvested and cultured in 10% FBS-containing RPMI. GM-CSF (500 ng/ml) (Novartis Pharma Basel, Switzerland) and IL-4 (500 U/ml) (Ono, Tokyo, Japan) were added on day 0. On day 7, cultured cells were collected as immature Mo-DCs. Immature Mo-DCs were further purified by negative selection with magnetic beads coated with mouse monoclonal anti-CD2, anti-CD3, and anti-CD19 antibodies (Dynabeads, Dynal, Oslo, Norway) as previously described but with minor modifications (Vartdal et al., 1987). This depletion procedure yielded greater than 90% CD14 −, CD80+, HLA-DR+ immature Mo-DCs.

2.2. CD4+ T cells

CD4+ T cells were purified from fresh human PBMCs with a CD4 + isolation kit (Dynabeads, Dynal) according to the manufacturer's instructions. The purity of CD4+ T cells was greater than 98% as analyzed with a FACS Calibur flow cytometer and CELLQuest software (Becton Dickinson, San Jose, CA).

2.3. Tumor cells and induction of necrosis

Human gastric carcinoma cell line GCTM-1 was maintained in 10% FBS-containing RPMI at 37 °C. Necrotic GCTM-1 cells were induced as previously described but with minor modifications (Nestle et al., 1998). In brief, tumor cells were washed with phosphate-buffered-saline (PBS) (Wako, Osaka, Japan) and then resuspended in RPMI. Cells were lysed by five cycles of freezing in liquid nitrogen and thawing at 37 °C. Lysis was monitored by light microscopy. Larger particles were removed by centrifugation. Whole cell lysates were mixed with collagen gel as tumor-associated antigens.

2.4. 3-D two-layer collagen gel culture model

Mo-DCs were used at 4×10^5 cells per assay and suspended in 20-μl RPMI containing with 1% human serum albumin (HSA). Mo-DCs were mixed with an equal volume of chilled type I collagen (Kokencellgen I-AC: 0.3%) (Funakoshi, Tokyo, Japan). The final collagen concentration was 0.15%. The mixture was transferred to 96-well plates (Nalge Nunc International) at 40 μl/well. Before the mixture was allowed to polymerize, a mixture of 20-μl RPMI with 1% HSA containing 4×10^5 necrotic GCTM-1 cells mixed with an equal volume of chilled type I collagen was layered onto the Mo-DC mixture. The two layers of mixture were then allowed to polymerize for approximately 1 h at 37 °C. After polymerization, 200-μl RPMI with 1% HSA was added to each well. A schematic of our culture model is shown in Fig. 1. These 3-D two-layer cultures were then incubated at 37 °C in a humidified atmosphere of 5% CO_2. Liquid culture medium was changed everyday and stored at −80 °C for later analyses. Mo-DCs suspended in the collagen matrix were observed by phase-contrast microscopy. Microscope was connected with digital camera, COOLPIX 950 (Nikon, Tokyo, Japan) and images were recorded in XGA-size (1024 × 768 pixels).

2.5. Time-lapse videomicroscopy

Dynamic cell motility was recorded as follows. Cells embedded within the collagen gel matrix were visualized on a phase-contrast microscope. The image was monitored on a screen of 15 inches monitor, 15ZR7 (Toshiba, Tokyo, Japan) and recorded with a digital video recorder, DCR-PC9 (Sony, Tokyo, Japan). We could focus on individual cells consecutively and also record time-lapse movements of individual cells. Furthermore, we could select certain images at will for further examination.

2.6. Cell viability

To evaluate cell viability, Mo-DCs existing in gel were stained with DNA-binding fluorochrome bis-

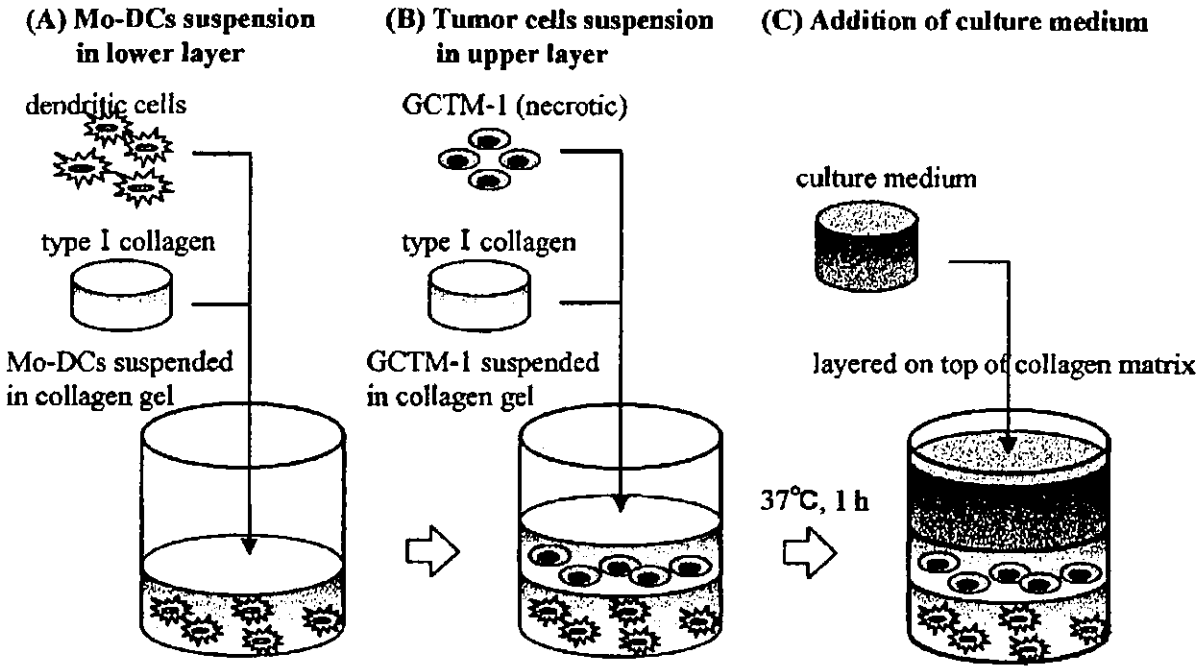

Fig. 1. Schematic of 3-D two-layer collagen matrix culture model. (A) Mo-DCs were suspended in 20-μl RPMI 1640 with 1% HSA. and mixed with an equal volume of chilled type I collagen. The mixture was transferred to 96-well plates at 40 μl/well. (B) Before the mixture containing Mo-DCs was allowed to polymerize, collagen gel containing tumor cells (made in the same way as the Mo-DCs mixture) was layered onto the DC mixture. (C) Two-layer collagen matrix was allowed to polymerize for approximately 1 h at 37 °C. After polymerization, 200-μl culture medium was added. This 3-D two-layer culture model was incubated at 37 °C in a humidified atmosphere of 5% CO_2 and observed with time-lapse microscopy.

benzimide stain (Hoechst 33342; Molecular Probes, Eugene, OR) and propidium iodide (PI; Molecular Probes). Briefly, 4×10^5 Mo-DCs were cultured in the mixture of RPMI with 1% HSA and type I collagen using 96-well plastic plate. Twenty microliters of Hoechst 33342 was added to culture medium at first and then incubated for 1 h at 37 °C. Next, 20 μl of PI was added to culture medium and incubated for 10 min at 37 °C. After these incubation times, fluorescence-positive cells were counted with a fluorescence microscope. Hoechst-positive and PI-negative cells were considered viable and PI-positive cells were considered nonviable. We calculated the ratio of a fluorescence-dyeing cell for 100 cells. Data were expressed as the mean ± S.D. of percent fluorescence-positive cells of eight independent wells.

2.7. Capture of necrotic GCTM-1 cells by Mo-DCs

Mo-DCs and necrotic GCTM-1 were labeled with PKH67 (green) and PKH26 (red) fluors (Sigma), respectively. Fluorescently-labeled Mo-DCs and necrotic GCTM-1 cells were embedded separately into collagen matrix and then observed by fluorescence microscopy. When images of Mo-DCs were superimposed with those of GCTM-1 cells, areas of co-localization appeared yellow or orange. Such cells were considered necrotic tumor-capturing Mo-DCs. Mo-DCs in the upper layer (migrating Mo-DCs) were counted in five upper fields (x200) at random. Percent phagocytosis represents the ratio of a tumor-capturing Mo-DC for total migrating Mo-DCs. Data were expressed as the mean ± S.D. of percent phagocytotic Mo-DC.

2.8. Collection of cells from 3-D two-layer collagen gel culture model

Mo-DCs were harvested from the collagen matrix by digestion with collagenase (Wako) as previously described but with minor modifications (Friedl et al., 1995). In brief, collagen matrix containing Mo-DCs was incubated with highly purified collagenase (final

concentration, 7500 U/ml) for 5 min. Cells were washed two times with PBS (Wako) and resuspended in RPMI for further study.

2.9. Expression of antigen-presentation-related molecules on Mo-DCs

To analyze the expression of antigen-presentation-related molecules on Mo-DCs, cells collected from collagen matrix were incubated for 1 h with one of the following monoclonal antibodies (BD Pharmingen, San Diego, CA) conjugated to FITC for direct staining: anti-CD83, anti-HLA-DR, or PE-anti-CD80, PE-anti-CD86. The isotype controls, IgG1 and IgG2, were also obtained from BD Pharmingen. For staining, cells were washed two times with PBS (Wako) and incubated in PBS containing 3% bovine serum albumin (BSA) (Sigma) and 0.1% NaN_3 (Sigma) (referred to as FACS buffer) and the appropriate concentration of labeled mAb for 1 h at 4 °C. After cells were washed with FACS buffer, the fluorescence intensities of gated Mo-DCs populations were measured with a FACS Calibur flow cytometer and analyzed with CELLQuest software (Becton Dickinson).

2.10. IL-12 and interferon-γ (IFN-γ) secretion

Culture supernatants were collected every 24 h and the concentrations of IL-12 p40 and interferon-γ (IFN-γ) were determined by enzyme-linked immunosorbent assay (ELISA) kits specific for IL-12 p40 and IFN-γ (Biosource, Camarillo, CA). ELISA protocols were described previously (Wilkinson et al., 1996). The detection limit of these ELISAs for IL-12 p40 is 2 pg/ml and for IFN-γ is 4 pg/ml.

3. Results

3.1. Morphology of Mo-DCs

Mo-DCs embedded in collagen gels (lower layer) were observed by phase-contrast microscopy. In collagen lattices, Mo-DCs extended processes from the cell

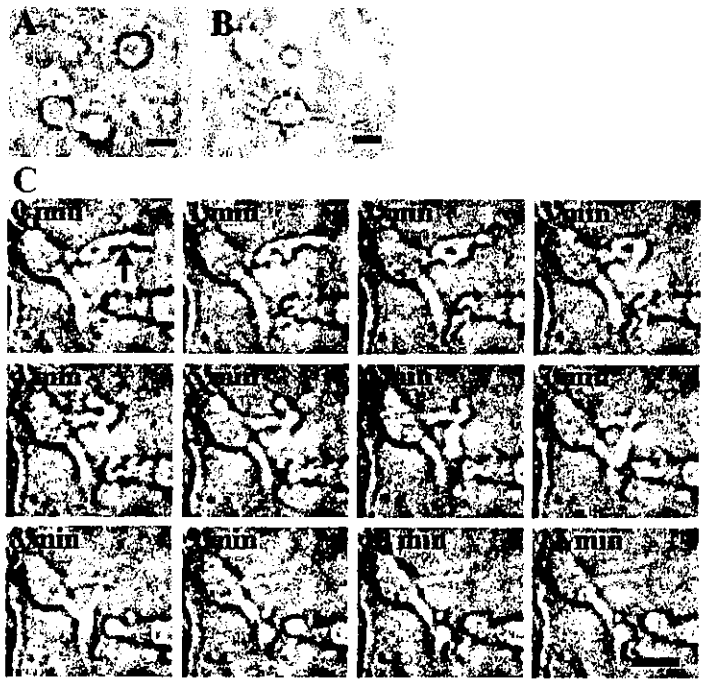

Fig. 2. Appearance of Mo-DCs in 3-D collagen matrix. Mo-DCs were cultured in collagen matrix for 7 days and were observed under phase-contrast microscopy. (A) Some Mo-DCs had a round shape right after cultivation in collagen matrix. (B) Most Mo-DCs extended processes in many directions on day 4. (C) Time-lapse analysis of dendrite formation by Mo-DC in collagen matrix. The formation of dendrites on day 4 was observed using time-lapse videomicroscopy. Dendrite (black arrow) showed continuous movement during observation. Images are shown at 1-min intervals. The time of the first image is arbitrarily set to 0 min. Magnification, ×400. Scale bars, 10 μm.

membrane that were characteristic within 24 h after initial culture. As shown in Fig. 2A, some Mo-DCs retained a round shape with many short processes. Some Mo-DCs changed to a spherical shape and extended several long "dendritic" processes that were 20- to 50-μm long (Fig. 2B).

Videomicroscopy revealed that Mo-DCs embedded in collagen gels developed considerable flexibility in cell shape. Dendrites on cell bodies repeatedly extended and retracted the processes/dendrites over the course of several minutes (Fig. 2C).

3.2. Survival of Mo-DCs

Immature Mo-DCs were generated from PBMCs by culture in medium containing GM-CSF and IL-4 for 7 days as described in Materials and methods. These immature Mo-DCs were embedded within collagen gel and cultured in RPMI containing 1% HSA for several weeks. Culture medium was changed every 24 h. Cells were observed by phase-contrast microscopy. On day 7, many Mo-DCs maintained multiple short processes or several long processes (Fig. 3A) and these cells seemed to be viable. As culture periods were extended, however, the number of Mo-DCs showing cellular fragmentation increased gradually (Fig. 3B). These Mo-DCs were considered as dead cells, probably apoptotic cells. To evaluate cell viability, Mo-DCs were stained with Hoechst 33342 and PI and evaluated with a fluorescent microscope as described in Materials and methods. Cells were alive until 7 days after the initial culture (day 7) and viable cells decreased gradually after day 9 (Fig. 3C, left panel). The percentage of viable cells on day 15 was $40.2 \pm 6.91\%$. On the other hand, nonviable cells increased gradually after day 9 and reached $59.6 \pm 6.12\%$ on day 15 (Fig. 3C, right panel). Most Mo-DCs appeared to be dead by day 21. The data are representative of five independent experiments using Mo-DCs generated from three different donors.

3.3. Migration and phagocytosis of Mo-DCs

When Mo-DCs and necrotic GCTM-1 were embedded in collagen gel (single-layer collagen gel culture), approximately 10% of Mo-DCs were active and migrated over a distance of 10 μm. Time-lapse videomicroscopy showed a Mo-DC migrating toward a necrotic GCTM-1 fragment that was about 30 μm away (Fig. 4). The Mo-DC then migrated to the GCTM-1 fragment, made contact with it, and engulfed it (phagocytosis) within 10 min.

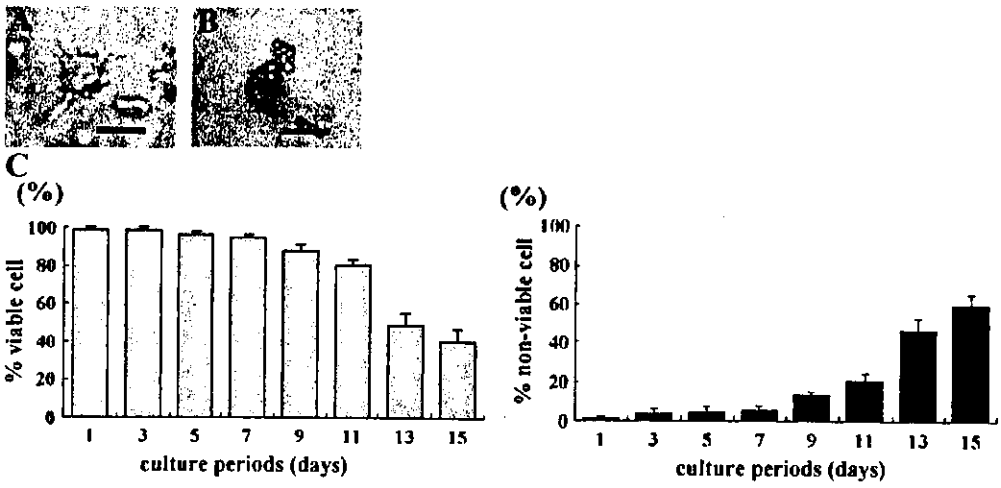

Fig. 3. Survival of Mo-DCs. Mo-DCs were cultured in collagen matrix and were observed under phase-contrast microscopy and fluorescence microscopy. (A) On day 7, most Mo-DCs had some processes and seemed to be still alive. Magnification, ×400. Scale bars, 10 μm. (B) On day 14, many Mo-DCs suddenly appeared fragment. These cells seemed to be dead. Magnification, ×400. Scale bars, 10 μm. (C) Cell viability was determined with Hoechst 33342 and PI staining as described in Materials and methods. Hoechst-positive and PI-negative cells were considered viable and PI-positive cells were considered nonviable. The data are representative of five independent experiments using Mo-DCs generating from three different donors. Data were expressed as the mean ± S.D. of percent fluorescence-positive cells of eight independent wells.

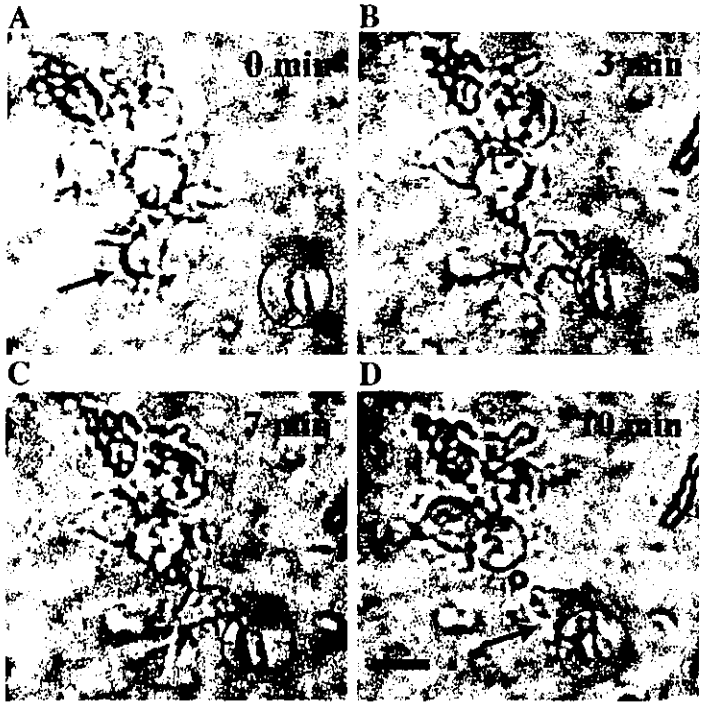

Fig. 4. Migration of and phagocytosis by Mo-DC in 3-D collagen gel culture. The Mo-DC migrated toward a necrotic tumor cell and phagocyted it over a time course of 10 min. (A) A cluster of Mo-DCs is visible in collagen matrix. (B, C) One (black arrows) moved spontaneously toward a fragment of necrotic GCTM-1 cell (black circle). (D) Ten minutes after initial observation, the Mo-DC reached the fragment and internalized it. Magnification, ×400. Scale bars, 10 μm.

With our two-layer collagen gel model, we were able to evaluate simultaneously both migratory and phagocytic abilities of Mo-DCs. For this purpose, Mo-DCs were labeled with the green fluorescent marker PKH67 and necrotic GCTM-1 were labeled with the red fluorescent marker PKH26. Fluorescently labeled cells were embedded separately in collagen gels. The lower collagen gel layer contained Mo-DCs (green), and the upper layer contained necrotic GCTM-1 (red). We then imaged this 3-D two-layer model by fluorescence microscopy (Fig. 5). On day 1 of culture, many Mo-DCs migrated from the lower layer to the upper layer, and some had engulfed necrotic GCTM-1 (yellow). In the first 24 h of incubation, 10% to 20% of Mo-DCs migrated into the upper layer. Percent phagocytosis was $13.2 \pm 3.03\%$ (Fig. 5E). Then the number of migrating Mo-DCs decreased after 24 h. In contrast, percent phagocytosis increased to $19.4 \pm 4.72\%$ at day 2 (Fig. 5E). The data are representative of three independent experiments using Mo-DCs generated from three different donors.

3.4. Expression of antigen-presentation-related molecules on Mo-DCs

Mo-DCs were embedded in collagen gel with or without necrotic GCTM-1. Seven days after initiation of culture, Mo-DCs were collected from collagen gels with collagenase, and the expression of antigen-presentation-related molecules such as HLA-DR, CD80, and CD86 was examined with FACS analysis. Mo-DCs cultured with necrotic GCTM-1 showed increased expression of HLA-DR, CD80, and CD86 in comparison with Mo-DCs cultured in the absence of necrotic GCTM-1 (Fig. 6). The data are representative of three independent experiments using Mo-DCs generated from three different donors.

3.5. IL-12 secretion by Mo-DCs

Using our 3-D two-layer collagen gel model, we investigated secretion of IL-12 and IFN-γ by Mo-DCs. Culture medium was changed every day and stored at -80 °C until assay. The concentration of

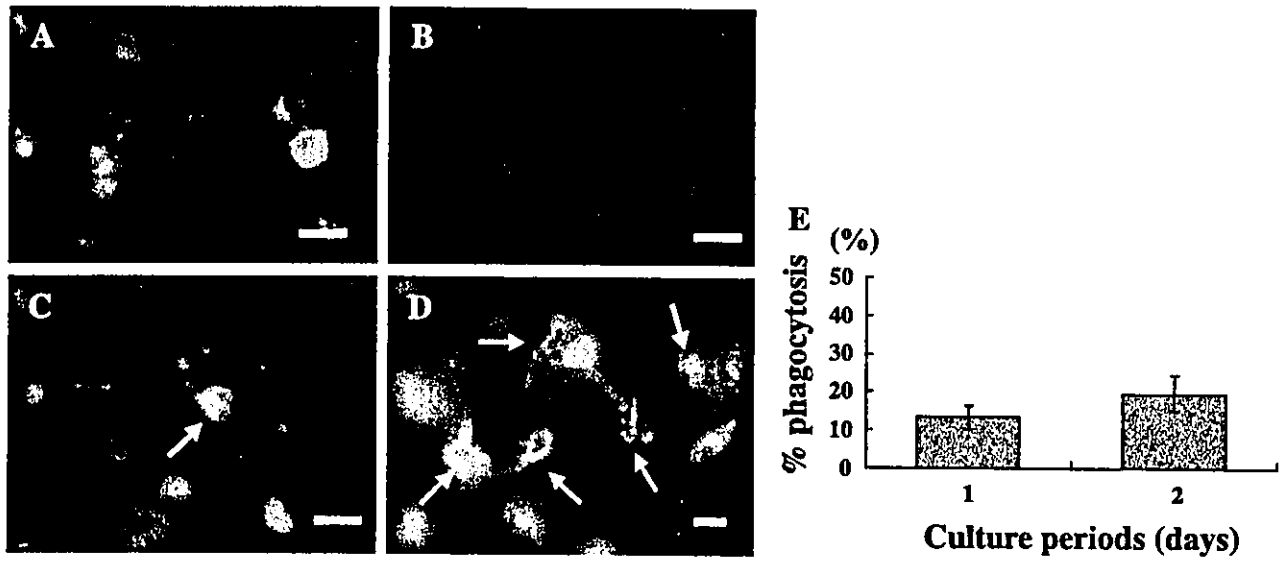

Fig. 5. Migration and phagocytosis of Mo-DCs in 3-D two-layer collagen matrix. This model consisted of two different layers of collagen gels. (A) The lower layer contained Mo-DCs labeled with PKH67 (green). (B) The upper layer contained necrotic GCTM-1 cells labeled with PKH26 (red). (C, E) Twenty-four hours after the initial cultivation (day 1), Mo-DCs migrated to the upper layer and were seen at the same field with tumor cells. Some of them appeared to be yellow cells (white arrow), implying phagocytosis of tumor cells by Mo-DCs. The percentage of phagocytosis on day 1 was 13.2 ± 3.03%. (D, E) Forty-eight hours after the initial cultivation (day 2), the number of Mo-DCs that had engulfed necrotic GCTM-1 had increased. The percentage of phagocytosis on day 2 was 19.4 ± 4.72%. Data represent the mean ± S.D. of five experiments. A representative experiment of three is shown. Magnification, ×200. Scale bars, 10 μm.

each cytokine represents roughly the daily secretion of each cytokine. When the upper layer contained necrotic GCTM-1, Mo-DCs secreted large amounts of IL-12 between days 3 and 5. Secretion of IL-12 decreased gradually from days 6 (Fig. 7A). To exclude a possibility that GCTM-1 themselves release IL-12, necrotic GCTM-1 alone were cultured in collagen matrix for 7 days. No IL-12 was detected in this culture condition. When the upper layer did not contain necrotic GCTM-1, IL-12 secretion was not detected during the 7 days of culture. IFN-γ was not detected regardless of the presence of necrotic GCTM-1 in the upper layer (data not shown).

When the upper layer contained both necrotic GCTM-1 and CD4+ T cells, the pattern of IL-12 secretion was very similar to that when the upper

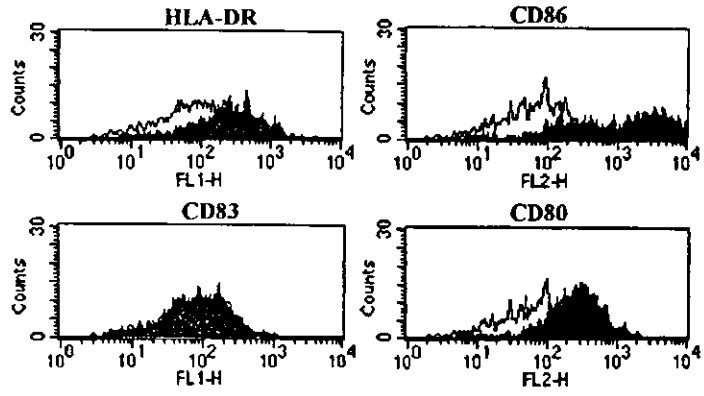

Fig. 6. Expression of antigen-presentation-related molecules on Mo-DCs in 3-D collagen gel. Cells were collected and analyzed on day 7. Mo-DCs cultured with necrotic GCTM-1 (shaded curves) showed increased expression of HLA-DR, CD86, and CD80 compared with Mo-DCs cultured without necrotic GCTM-1 (solid curves). The data are representative of three independent experiments using Mo-DCs generated from three different donors.

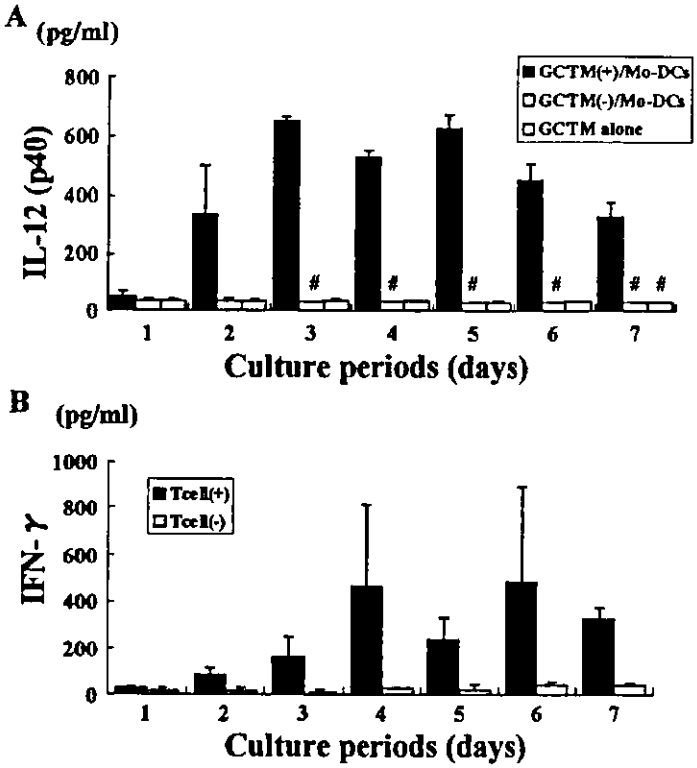

Fig. 7. Cytokine secretion by Mo-DCs in 3-D two-layer culture model. The supernatants were collected daily from 3-D two-layer collagen gel culture that contained Mo-DCs in the lower layer. (A) When the upper layer contained necrotic GCTM-1 [GCTM(+)/Mo-DCs], IL-12 p40 secretion was detected from days 1 to 7. In contrast, IL-12 p40 secretion was barely detected when the upper layer lacked necrotic GCTM-1 [GCTM(−)/Mo-DCs]. When the lower layer did not contain Mo-DCs [GCTM alone], IL-12 p40 secretion was not detected. (B) [T cell(−)] represents that the upper layer contains necrotic GCTM-1 alone. [T cell(+)] represents that the upper layer contains both necrotic GCTM-1 and CD4+ T cells. Cytokine concentration represents mean ± S.D. of three wells. The data are representative of three independent experiments using Mo-DCs generated from three different donors. This figure was obtained from a simultaneous experiment using Mo-DCs generated from the same donor.

layer contained only necrotic GCTM-1 (data not shown). Under this culture condition, IFN-γ secretion was detected and continued until at least day 7 (Fig. 7B). The data are representative of three independent experiments using Mo-DCs generated from three different donors. Fig. 7 was obtained from a simultaneous experiment using Mo-DCs generated from the same donor.

3.6. Dynamics of the interaction between Mo-DCs and T cells

As described above (Fig. 2), Mo-DCs embedded within collagen gels showed considerable flexibility in cell shape. Using time-lapse videomicroscopy, we observed individual interactions between Mo-DCs and T cells.

4. Discussion

We describe here results from our experiments with a novel 3-D two-layer collagen gel culture system that can be used to evaluate and monitor Mo-DCs used as vectors for DC-vaccine therapies. With this model system, we were able to evaluate simultaneously multiple functions of Mo-DCs, including migration, phagocytosis of necrotic tumor cells, and interactions with T cells, in real time with phase-contrast or fluorescence microscopy. In addition, we could also observe dynamic cell–cell interactions on a single-cell basis with time-lapse videomicroscopy.

Recent advances in medical technology have made it possible to develop 3-D DC culture systems that are similar to in vivo environments. Hydrated

collagen gel has been used in 3-D cell culture systems, because the structure of collagen lattices resembles that of several tissues, including dermis and the network-like stroma of lymph node (Friedl and Brocker, 2000). Gunzer et al. (1997, 2000a,b) have reported data that support the usefulness of 3-D collagen matrix systems in the study of in vivo-like DC behaviors, especially migration and DC–T cell interactions. Murine epidermal Langerhans cells and bone marrow DCs were used as target cells and embedded in collagen lattices for analysis on an inverted confocal scanning microscope. Gunzer et al. (1997, 2000a,b) showed that DCs formed extended membrane processes, which are characteristic of these cells. They recently described a modified method by which migration of murine DCs within 3-D collagen lattices can be analyzed by time-lapse videomicroscopy and computer-assisted single-cell tracking. These in vitro models certainly inform us of missing in vivo behavior of DCs. In the present study, we focused on the development of a method that allows easy and simultaneous evaluation of multiple functions of Mo-DCs. It is generally accepted that DCs play many roles in induction of specific T cell immunity in vivo. It is thought that DCs migrate to, capture, and then process antigens, move to T cell-dependent areas of secondary lymphoid organs, and stimulate naïve T cells (Banchereau and Steinman, 1998; Banchereau et al., 2000). On the basis of these functions, we developed a new 3-D two-layer collagen gel culture system. Each layer is almost 1.2-mm thick. In our system, Mo-DCs and necrotic tumor cells exist separately in different collagen gel layers. To capture necrotic GCTM-1, Mo-DCs must migrate to the upper layer. If the upper layer contains T cells, migrating Mo-DCs can make contact with T cells in the upper layer. In our system, 10% to 20% of Mo-DCs migrated from the lower layer to the upper layer within 24 h of incubation, and more than half of the migrating Mo-DCs engulfed necrotic GCTM-1 by day 2 (Fig. 5). Consistent with data from experiments with 2-D culture systems (Labeur et al., 1999; Hochrein et al., 2000; Liu, 2001; Schnurr et al., 2001), we observed in our 3-D culture system that Mo-DCs that capture GCTM-1 secrete high level of IL-12 (Fig. 7A). When the upper layer did not contain necrotic GCTM-1, IL-12 was not detected in culture media. In addition, IL-12 secretion was detected after but not before Mo-DCs appeared in the upper layer (data not shown). Because IFN-γ production was detected only when the upper layer contained CD4+ T cells, IFN-γ may be secreted primarily by CD4+ T cells (Fig. 7). Since it has been shown that IL-12 can induce IFN-γ production in CD4+ T cells (Gerosa et al., 1996; Kuroki et al., 2003), we examined if IL-12 secreted from GCTM-1-capturing Mo-DCs induces IFN-γ in CD4+ T cells existing in the upper layer of our model. As shown in Fig. 7B, IFN-γ secretion occurred only when CD4+ T cells coexisted with necrotic GCTM-1 in the upper layer. In addition, IFN-γ secretion was always followed by IL-12 secretion (Fig. 7A), CD4+ T cells alone in the upper layer or Mo-DCs alone in the lower layer did not produce detectable IFN-γ (data not shown). These results suggest that Mo-DCs migrate toward necrotic GCTM-1, captured them, and secreted IL-12 and that Mo-DC-secreting IL-12 induced IFN-γ in CD4+ T cells.

In 3-D one-layer culture systems, investigators observed that Mo-DCs survive at least 2 weeks within collagen lattices and that Mo-DCs that captured necrotic GCTM-1 showed increased the expression of HLA-DR, CD80, and CD86, which are important for antigen presentation and stimulation of naïve T cells (Liu, 2001; Mellman and Steinman, 2001; Thery and Amigorena, 2001). Expression of these molecules was elevated even on day 7 of incubation (Fig. 6).

In conclusion, using this 3-D two-layer collagen matrix model, we could easily evaluate a series of in vivo-like Mo-DC functions in the antigen presentation process in real time. In addition, we could observe cell interactions on an individual basis by time-lapse videomicroscopy. We are now beginning to use this two-layer collagen gel system for evaluation of the quality of and monitoring of Mo-DCs.

Acknowledgements

This study was supported by a Grant-in-Aid for General Scientific Research (13470240) from the Ministry of Education, Culture, Sports, Science, and Technology of Japan.

We thank Kaori Nomiyama and Takaaki Kanemaru for their skillful technical assistance.

References

Banchereau, J., Steinman, R.M., 1998. Dendritic cells and the control of immunity. Nature 392, 245.

Banchereau, J., Briere, F., Caux, C., Davoust, J., Lebecque, S., Liu, Y.J., Pulendran, B., Palucka, K., 2000. Immunobiology of dendritic cells. Annu. Rev. Immunol. 18, 767.

Banchereau, J., Schuler-Thurner, B., Palucka, A.K., Schuler, G., 2001. Dendritic cells as vectors for therapy. Cell 106, 271.

Cella, M., Sallusto, F., Lanzavecchia, A., 1997. Origin, maturation and antigen presentation function of dendritic cells. Curr. Opin. Immunol. 9, 10.

Dallal, R.M., Lotze, M.T., 2000. The dendritic cell and human cancer vaccines. Curr. Opin. Immunol. 12, 583.

Fong, L., Engleman, E.G., 2000. Dendritic cells in cancer immunotherapy. Annu. Rev. Immunol. 18, 245.

Friedl, P., Brocker, E.-B., 2000. The biology of cell locomotion within three-dimensional extracellular matrix. Cell. Mol. Life Sci. 57, 41.

Friedl, P., Noble, P.B., Zanker, K.S., 1993. Lymphocyte locomotion in three-dimensional collagen gels. Comparison of three quantitative methods for analysing cell trajectories. J. Immunol. Methods 165, 157.

Friedl, P., Noble, P.B., Zanker, K.S., 1995. T lymphocyte locomotion in a three-dimensional collagen matrix: expression and function of cell adhesion molecules. J. Immunol. 154, 4973.

Friedl, P., Entschladen, F., Conrad, C., Niggemann, B., Zanker, K.S., 1998. $CD4^+$ T lymphocytes migrating in three-dimensional collagen lattices lack focal adhesions and utilize β1 integrin-independent strategies for polarization, interaction with collagen fibers and locomotion. Eur. J. Immunol. 28, 2331.

Gerosa, F., Paganin, C., Peritt, D., Paiola, F., Scupoli, M.T., Aste-Amezaga, M., Frank, I., Trinchieri, G., 1996. Interleukin-12 primes human CD4 and CD8 T cell clones for high production of both interfefon-γ and interleukin-10. J. Exp. Med. 183, 2559.

Gunzer, M., Kampgen, E., Brocker, E.-B., Zanker, K.S., Friedl, P., 1997. Migration of dendritic cells in 3D-collagen lattices: visualization of dynamic interactions with the substratum and the distribution of surface structures via a novel confocal reflection imaging technique. Adv. Exp. Med. Biol. 417, 97.

Gunzer, M., Friedl, P., Niggemann, B., Brocker, E.-B., Kampgen, E., Zanker, K.S., 2000a. Migration of dendritic cells within 3-D collagen lattices is dependent on tissue origin, state of maturation, and matrix structure and is maintained by proinflammatory cytokines. J. Leukoc. Biol. 67, 622.

Gunzer, M., Schafer, A., Borgmann, S., Grabbe, S., Zanker, K.S., Brocker, E.-B., Kampgen, E., Friedl, P., 2000b. Antigen presentation in extracellular matrix: interactions of T cells with dendritic cells are dynamic, short lived, and sequential. Immunity 13, 323.

Hochrein, H., O'Keeffe, M., Luft, T., Vandenabeele, S., Grumont, R.J., Maraskovsky, E., Shortman, K., 2000. Interleukin (IL)-4 is a major regulatory cytokine governing bioactive IL-12 production by mouse and human dendritic cells. J. Exp. Med. 192, 823.

Kuppner, M.C., Gastpar, R., Gelwer, S., Nossner, E., Ochmann, O., Scarner, A., Issels, R.D., 2001. The role of heat shock protein (hsp70) in dendritic cell maturation: (hsp70) induces the maturation of immature dendritic cells but reduces DC differentiation from monocyte precursors. Eur. J. Immunol. 31, 1602.

Kuroki, H., Morisaki, T., Matsumoto, K., Onishi, H., Baba, E., Tanaka, M., Katano, M., 2003. Streptococcal preparation OK-432: a new maturation factor of monocyte-derived dendritic cells for clinical use. Cancer Immunol. Immunother. 52, 561.

Labeur, M.S., Roters, B., Pers, B., Mehling, A., Luger, T.A., Schwarz, T., Grabbe, S., 1999. Generation of tumor immunity by bone marrow-derived dendritic cells correlates with dendritic cell maturation stage. J. Immunol. 162, 168.

Lanzavecchia, A., Sallusto, F., 2001. Regulation of T cell immunity by dendritic cells. Cell 106, 263.

Liu, Y.J., 2001. Dendritic cell subsets and lineages, and their functions in innate and adaptive immunity. Cell 106, 259.

Mellman, I., Steinman, R.M., 2001. Dendritic cells: specialized and regulated antigen processing machines. Cell 106, 255.

Nakamura, K., Kuga, H., Morisaki, T., Baba, E., Sato, N., Mizumoto, K., Sueishi, K., Tanaka, M., Katano, M., 2002. Simulated microgravity culture system for a 3-D carcinoma tissue model. BioTechniques 33, 1068.

Nestle, F.O., Alijagic, S., Gilliet, M., Sun, Y., Grabbe, S., Dummer, R., Burg, G., Schadendorf, D., 1998. Vaccination of melanoma patients with peptide-or tumor lysate-pulsed dendritic cells. Nat. Med. 4, 328.

Onishi, H., Morisaki, T., Baba, E., Kuga, H., Kuroki, H., Matsumoto, K., Tanaka, M., Katano, M., 2002. Dysfunctional and short-lived subsets in monocyte-derived dendritic cells from patients with advanced cancer. Clin. Immunol. 105, 286.

Reinhard, G., Marten, A., Kiske, S.M., Feil, F., Bieber, T., Schmidt-wolf, I.G., 2002. Generation of dendritic cell-based vaccines for cancer therapy. Br. J. Cancer 86, 1529.

Sallusto, F., Lanzavecchia, A., 1994. Efficient presentation of soluble antigen by cultured human dendritic cells is maintained by granulocyte/macrophage colony-stimulating factor plus interleukin 4 and downregulated by tumor necrosis factor alpha. J. Exp. Med. 179, 1109.

Schnurr, M., Galambos, P., Scholz, C., Then, F., Dauer, M., Endres, S., Eigler, A., 2001. Tumor cell lysate-pulsed human dendritic cells induce a T-cell response against pancreatic carcinoma cells: an in vitro model for the assessment of tumor vaccines. Cancer Res. 61, 6445.

Schuler, G., Schuler-Thurner, B., Steinman, R.M., 2003. The use of dendritic cells in cancer immunotherapy. Curr. Opin. Immunol. 15, 138.

Thery, C., Amigorena, S., 2001. The cell biology of antigen presentation in dendritic cells. Curr. Opin. Immunol. 13, 45.

Thomas, R., Chambers, M., Boytar, R., Baker, K., Cavanagh, L.L., MacFadyen, S., Smithers, M., Jenkins, M., Anderson, J., 1999. Immature human monocyte-derived dendritic cells migrate rapidly to draining lymph nodes after intradermal injection for melanoma immunotherapy. Melanoma Res. 9, 474.

Thurner, B., Haendle, I., Roder, C., Dieckmann, D., Keikavoussi, P., Jonuleit, H., Bender, A., Maczek, C., Schreiner, D., von den Driesch, P., Brocker, E.B., Steinman, R.M., Enk, A., Kampgen, E., Schuler, G., 1999. Vaccination with mage-3A1 peptide-

pulsed mature, monocyte-derived dendritic cells expands specific cytotoxic T cells and induces regression of some metastases in advanced stage IV melanoma. J. Exp. Med. 190, 1669.

Vartdal, F., Kvalheim, G., Lea, T., Bosnes, V., Gaudernack, G., Ugelstad, J., Albrechtsen, D., 1987. Depletion of T lymphocytes from human bone marrow: use of magnetic monosized polymer microspheres coated with T lymphocyte specific monoclonal antibodies. Transplantation 43, 366.

Wilkinson, V.L., Warrier, R.R., Truitt, T.P., Nunes, P., Gately, M.K., Presky, D.H., 1996. Characterization of anti-mouse IL-12 monoclonal antibodies and measurement of mouse IL-12 by ELISA. J. Immunol. Methods 189, 15.